PHOTONS AND ELECTRONS STUDIES AT CMS

C. ROVELLI, on behalf of the CMS Collaboration
Università La Sapienza and INFN Roma1,
P.le Aldo Moro 2, 00185 Roma, Italy

Reconstructing electrons and photons with high efficiency and good momentum resolution is crucial for many physics channels at the CMS experiment. This goal is challenging in view of the high material budget in front of the electromagnetic calorimeter and the presence of a strong magnetic field. The reconstruction algorithms are described here. The use of data from the first proton-proton collisions recorded by CMS at the center of mass energy of 900 GeV to commission the reconstruction of electrons and photons is discussed.

1 Introduction

CMS is one of the two multipurpose experiments collecting data at the Large Hadron Collider at CERN. The LHC started the data taking at the end of 2009 providing the experiments proton-proton collisions at the centre-of-mass energies of 0.9 and 2.36 TeV. Data at $\sqrt{s}$=7 TeV have been collected starting in 2010.
The detection of electrons and photons is of primary importance at the LHC as these particles characterize the final state for many SUSY or extra dimensions scenaria, Higgs decay channels and Standard Model processes. Several reconstruction tools have been developed in recent years and are currently being tested with collision data. Data collected at $\sqrt{s}$=900 GeV have been used to check the basic ingredients contributing to the reconstruction and identification of electromagnetic physics objects and to compare them with the simulation. Given the low integrated luminosity the study has been performed without identification requirements. Most of the reconstructed candidates are therefore due to fakes and the comparison is mainly carried out for background [1].

2 The CMS detector

A detailed description of the CMS detector can be found in [2]. The central feature of the CMS apparatus is a superconducting solenoid of 6 m internal diameter, providing an uniform magnetic field of 3.8 T. Within the magnetic field are the tracker, the electromagnetic calorimeter and the brass/scintillator hadron calorimeter. Gas-based detectors embedded in the steel return yoke are used to measure muons.
A crucial role in the electron and photon measurement is played by the electromagnetic calorimeter (ECAL) and the tracker. ECAL is a homogeneous calorimeter made of 75848 lead tungstate scintillating crystals. It consists of a central barrel covering the pseudorapidity region up to $|\eta|$=1.5; the coverage for precision measurements extends up to $|\eta|$=2.6 including two endcaps.

A silicon preshower detector also covers the region between $|\eta|$=1.6 and $|\eta|$=2.6.
The tracker is made of 1440 silicon-pixel and 15148 silicon-strip detector modules and measures charged particles trajectories within the pseudorapidity range $|\eta|$ <2.5. The pixel tracker consists of three barrel layers and two endcap disks on each side of the barrel section. The barrel layers are located at a radius of 4.4 cm, 7.3 cm and 10.2 cm respectively.

3 Event selection

The results discussed here use about 200k minimum bias events recorded at $\sqrt{s}$=900 GeV in 2009. The events are selected by a trigger signal in any of the scintillator planes located in front of the Hadron Calorimeter Forward detectors (BSC). From these sample, collision events are selected offline by requiring them to be in time with a valid beam crossing measured by the coincidence of the two beam pickup monitors. The absence of a beam halo trigger, the presence of at least one hit with energy greater than 2 GeV in each of the Forward Hadron calorimeter detectors and a high fraction (>25%) of high purity tracks are also requried. Finally at least one primary vertex must be reconstructed in the event.
Collision data are compared to a full Monte Carlo simulation based on Geant4 of minimum bias events. The simulation is carried out using mis-alignments, mis-calibrations and dead channel lists corresponding to the startup conditions of the CMS detector.

4 Energy clustering

The reconstruction of electrons and photons starts by the detection of energy clusters in the electromagnetic calorimeter. Electromagnetic showers deposit their energy in several ECAL crystals. The presence of material in front of the calorimeter results in electron bremsstrahlung and photon conversions and because of the strong magnetic field the energy reaching the calorimeter is spread in ϕ. The energy is therefore clustered at the ECAL level by building a cluster of clusters (supercluster), which is extended in ϕ to minimize the cluster containment variations [3]. The clustering threshold is approximately 1 GeV in transverse energy E_T. Containment variations are corrected for as a function of energy and pseudorapidity using functions which can be extracted from data.
Kinematic and shower shape variables have been compared in data and Monte Carlo for superclusters in the ECAL fiducial region with E_T greater than 2 GeV. In total 3226 superclusters satisfying these requirements have been reconstructed in data, of which about 2/3 in the barrel. A good agreement is observed between data and simulation for all the considered variables, including clusters in the preshower detector. As an example, Fig.1 on the left shows the distribution in the barrel of $R9$, the ratio of the energy contained in the 3x3 region around the seed crystal and the total supercluster energy. $R9$, which is used to discriminate between converted and unconverted photons, can be larger than one due to fluctuations in the electronic noise.

5 Electron reconstruction

Electrons are characterized by the presence of a charged track pointing to the electromagnetic supercluster. Two different algorithms are used in CMS at the track seeding stage. In the ECAL driven seeding, roads are built from the supercluster to search for hits in the innermost part of the tracker. This algorithm is optimised for isolated electrons in the p_T range relevant for Z or W decays down to ∼5 GeV/c. It is complemented by the tracker driven seeding, which starts from hits in the tracker and is more suitable for low p_T and not isolated electrons.
As the bremsstrahlung radiation severely affects the track propagation, a dedicated tuning of the trajectory building and a Gaussian Sum Filter [4] track fit are used to well follow the non Gaussian

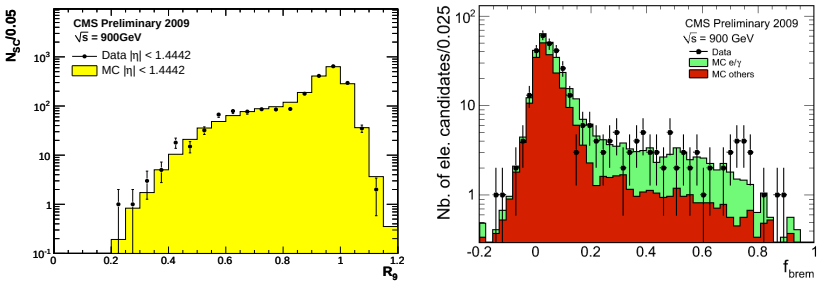

Figure 1: Left: Ratio between the energy contained in the 3x3 region around the seed crystal and the total supercluster energy for barrel superclusters. Right: Relative difference between the track momentum estimate at the innermost and at the outermost position. The Monte Carlo expectation for electron candidates matched to a generated electron or photon is also shown (filled green histogram). In both figures: The black dots correspond to data and the filled histogram to simulated minimum bias events. The Monte Carlo is normalized to the total number of candidates observed in data.

tails in the energy loss. As a result, the track hits can be collected up to the ECAL front face and this allows to obtain an unbiased estimate of the track momentum at both track ends. This procedure also gives a tracker measurement of the fraction of energy lost by bremsstrahlung ($fbrem$), defined as the relative difference between the momentum at the vertex and the momentum at the last point. Based on $fbrem$, different track-cluster patterns are defined and used to derive specific corrections as well as estimates of the electron quality [5].
In the collected minimum bias events only very low p_T electrons are expected and the sample of electron candidates is dominated by charged hadrons or electrons coming from photon conversions. In total 351 electron candidates have been reconstructed in data, of which about 2/3 in the barrel. Being at low p_T most of the candidates are reconstructed from the tracker driven algorithm; the relative fraction of electron candidates found by the two algorithms is well reproduced by the simulation. Several quantities used in the electron reconstruction have been compared between data and Monte Carlo. As an example, Fig.1 on the right shows the $fbrem$ distribution for the electron candidates, which is peaked at $fbrem$=0 since most of the candidates are fakes. A discrepancy in this variable would mean problems in the behaviour of the GSF algorithm or in the parameterization of the tracker material budget. The agreement between data and Monte Carlo is good. In general a good agreement is observed for all the considered variables.

6 Electromagnetic objects identification and isolation

At reconstruction level some cuts are applied in the seeding step and a first candidate preselection is done. Further electron identification is then achieved using shower shape variables and refined track-cluster matching. Electron classes based on the different observed patterns can be used to optimize the electron identification using probability distributions per class.
Isolation requirements can be imposed to suppress the QCD background. A simple and powerful isolation criterion comes from tracks originating from a common vertex as the electron. Also, the sum of the transverse energy reconstructed in ECAL individual channels or in HCAL towers around the reconstructed candidate can be used.
Isolation and shower shape variables for supercluster candidates can also be used for photon isolation and identification. All the checked isolation and identification variables show a good agreement between data and simulation.

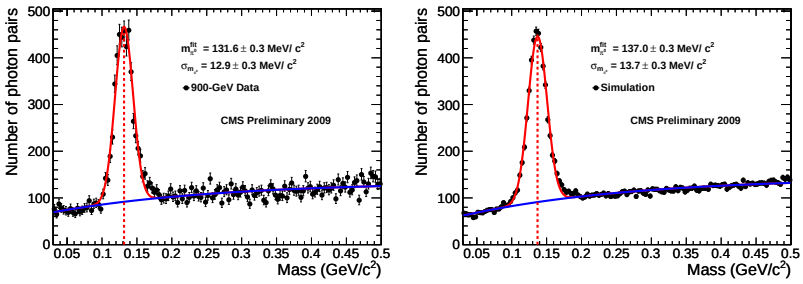

Figure 2: Photon-pair invariant-mass distribution ($|\eta|$ <1) in data (left) and Monte Carlo (right). Also shown is a fit of the π^0 mass peak by a Gaussian (red line). The fit mean value and resolution are 131.6±0.3 and 12.9±0.3 MeV/c^2 respectively for the data and 137.0±0.3 and 13.7±0.3MeV/c^2 for the simulation. The combinatorial background is fit by an exponential function (blue line).

7 Reconstruction of electromagnetic objects with the first LHC data

Resonances decaying into two photons have been searched for in the first collision data. A clear π^0 peak was observed just after few days, proving the good understanding of the detector. The η peak has been also observed and the π^0/η yields ratio measured in data is in good agreement with the one in the simulation. Due to the combined effect of not containment and readout thresholds the peak is expected to be at a value somehow lower than the real one. The shift in mass is well reproduced in the simulation, such as the peak width and the signal-to-background ratio. The uncorrected π^0 and η peaks are currently being used for the calibration of the electromagnetic calorimeter from data.
For physics studies Monte Carlo-based corrections determined from simulated single photons have been applied to the cluster energies. The photon-pair invariant mass distribution for candidates reconstructed within $|\eta|$ <1 is shown in Fig. 2 for data and Monte Carlo. The agreement for the measured mass value with the world average is within 2%, demonstrating the suitability of the simulation-based absolute ECAL cluster calibration for low-energy photons [6].

8 Summary

Using the first proton-proton collision data collected with the CMS detector at $\sqrt{s}$ =900 GeV many quantities entering the reconstruction of electromagnetic objects have been compared between data and Monte Carlo. Due to the limited statistics the comparison has been done without identification requirements, so the sample is dominated by background. All the considered variables show a good agreement between data and Monte Carlo, leading to the conclusion that the response of the subdetectors is well modeled in the simulation and that the algorithms behavior is consistent with expectations. The commissioning of the electromagnetic physics objects is continuing with the new LHC data at higher center of mass energy.

References

1. CMS Collaboration, CMS-PAS-EGM-10-001
2. CMS Collaboration, JINST 3 (2008) S08004.
3. CMS Collaboration, CERN-LHCC-2006-001 (2006).
4. W. Adam et al., J. Phys. G: Nucl. Part. Phys. 31 (2005) N9-N20
5. S. Baffioni et al., Eur. Phys. J. C 49 (2007).
6. CMS Collaboration, CMS-PAS-PFT-10-001